Some recent developments in understanding auroral electron acceleration processes

A. Olsson and P. Janhunen,

***Abstract*— Discrete auroral arcs and the associated inverted-V type electron precipitation are accompanied by potential structures, upgoing ion beams and plasma density depletions in the acceleration region altitude and above. However, exactly how these phenomena depend on altitude in various Kp and solar illumination conditions as well as at various magnetic local time (MLT) and invariant latitude (ILAT) is not so well known. We review the main results of our recent large statistical studies of the altitude dependence of these parameters using Polar data. We also include similar statistical results on some additional parameters that appear to have major importance in inverted-V auroral acceleration. These parameters include middle-energy (∼50-500 eV) electron anisotropies, certain types of electrostatic wave bursts as well as ion shell distributions. One of the most interesting results of the statistical studies is that many of the parameters mentioned change their behaviour rather abruptly at around 4 R_E radial distance. We draw the conclusion that the region for auroral energisation processes seem to take place within a closed potential structure below ∼3-4 R_E. These conclusions lead to a new scenario for auroral plasma physics and the energy flow in the auroral acceleration process. The observational results are in agreement with simulations that we also summarise in this paper.**

***Index Terms*— auroral electron acceleration, auroral potential structure, ionosphere-magnetosphere coupling.**

I. Introduction

AN auroral arc is a central element of ionosphere-magnetosphere coupling. Thus, in order to understand ionosphere-magnetosphere coupling more profoundly one should know the physical mechanisms responsible for auroral arcs.

Already 50 years ago [1] theoretically postulated the existence of parallel electric fields which could accelerate auroral electrons downward and ions upward from Earth. Soon thereafter, one could observe from rocket and satellite measurements convergent electric fields [27], [35] simultaneously with downward accelerated electrons and upward accelerated ions. Data from low-orbiting satellites showed an inverted-V like spectra of accelerated electrons. [10], [11]. The low and mid-altitude satellite observations (1000-14000 km) resulted in a model of the acceleration region as a U-shaped potential geometry (see Figure 1) [8] where the "bottom" of the U corresponds to the region of the parallel electric field. The closure of the potential structure and the generation mechanism has usually been assumed to take place in the opposite hemisphere or far out in the magnetotail. The physical mechanisms for generating the upward parallel electric field has been proposed with theories of double layers [5], [26], anomalous resistivity [32] or magnetic mirror force [2]. To be able to confirm or refute some of the proposed theories, a full understanding of the complete geometry of the potential is needed.

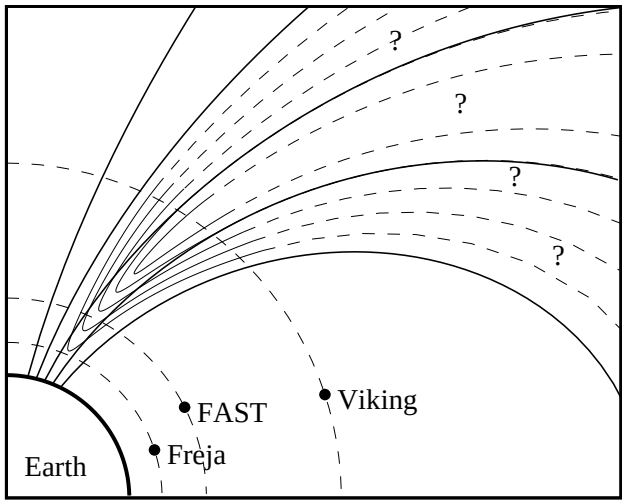

Fig. 1. Low-altitude satellite data suggest that the bottom of the potential structure is U-shaped. How the potential continues to higher altitudes is not constrained by these satellites, however.

To get some information about the closure of the U-shaped potential structure the electric field data for 65 auroral passes at ∼4 R_E altitude was studied with the Polar satellite [14]. A lack of convergent electric fields at high altitude was found. To explain this, the idea of a negative O-shaped potential well was introduced, i.e a potential model where the bottom part in all respect is the same as the traditional acceleration region of the U-shaped model, but which closes already below ∼4 R_E. In the closed potential model there is thus another region of downward parallel electric fields at a higher altitude (presumably 2-4 R_E). The net result of particles going through such a closed potential structure would be zero acceleration.

However, in [16] a correlation between waves and anisotropy of electrons was observed simultaneously with satellite crossings over various arcs and the energisation mechanism of electrons was suggested to be related to the broadband wave bursts. Acceleration of electrons due to waves alone (no potential drop), possibly lower-hybrid waves, has been proposed before [6], [3].

In a test particle simulation [15] the idea of a self-consistent "Cooperative Model" (CM) was developed, i.e a model of the acceleration process where both the closed potential structure in cooperation with wave-particle interaction takes place.

Manuscript received March 1, 2003; revised SOMETIME, 2003. This work was supported by the Swedish Research Council and the Academy of Finland.

A. Olsson is with the Swedish Institute of Space Physics.

P. Janhunen and H.E.J. Koskinen are with the Finnish Meteorological Institute.

The plasma waves would push the electrons up an electron potential hill at ∼3-4 R_E and the upper part of the potential structure work as an energisation region for the particles while the bottom part acts as the traditional acceleration region. The waves are thus the engine and the potential structure is the wheels and gear. The CM is discussed in detail in [17], [18] and in subsection VI.A of this paper.

To revisit the question about closure altitude of the potential structure in a more thorough way, a larger dataset and a complete altitude coverage would be needed. In order to also discuss the physical mechanisms maintaining the potential structure and the energy flow, information about the other arc-associated parameters is needed, for example observations of the altitude profiles of ion beams, cavities and waves. The Polar satellite has the advantage of covering the large altitude range (5000-32000 km) without gaps and thus we can study the altitude dependence of various arc-associated parameters during several years (1996-2001). It is important to also study the altitude dependence in different magnetic local time (MLT) sectors as well as different Kp conditions, invariant latitudes (ILAT), season and solar cycle conditions. We will in this paper review our latest results regarding the altitude profile of the arc-associated parameters. In this paper we will also summarise results concerning the altitude profile of other related parameters, i.e. the middle-energy anisotropy of electrons and ion shell distributions. We believe that these might also play a significant role in the auroral scenario. The observational results are section V (Simulations) then compared with a a hybrid simulation model for a stable arc. In a two-dimensional electrostatic simulation (subsection V.B) it is also shown that ion shell distributions can contain enough free energy for waves that could power electron energisation in the auroral process.

II. Instruments and datasets

We use 3-5 years of Polar data to study the altitude dependence of the occurrence frequency of auroral potential structures, upgoing ion beams, density depletions, electrostatic wave bursts, anisotropy of electrons and ion shells.

The potential structures are found by locating local minima in the plasma potential which is found by integrating the measured electric field from the EFI instrument [13] along the spacecraft orbit. The dataset of the electric fields during the years 1996-2001 covers the altitude range 5000-30000 km. The same dataset is used for studying the waves as well. Density depletions are studied by thresholding the Polar/EFI spacecraft potential during the years 1996-2000 (5000-30000 km altitude).

Ion beams are detected from Polar/TIMAS [37] during the years 1996-1998 and the data cover the altitude ranges 5000-10000, 20000-30000 km. To get a complete altitude coverage DE-1/EICS [36], data during the years 1981-1991 are also included. DE-1/EICS covers the altitudes 8000-23000 km during the 10 years. The ion shell distributions are also measured with Polar/TIMAS.

The anisotropy of electrons is studied with the Polar/HYDRA instrument [34] during the years 1996-2000 (5000-30000 km altitude).

The magnetic field experiment (MFE) is needed to decompose E-field into parallel and perpendicular components [33]

III. Statistical results of arc-associated parameters

This section is a condensed exposition of recent statistical studies. A reader not too interested in the details may safely skip to section IV.

As mentioned above, to obtain observational information about the physics of auroral acceleration processes, altitude profiles of the arc-associated physical quantities are of utmost importance. However, lacking satellite missions especially designed for producing magnetic conjunctions, instantaneous altitude profiles are impossible to obtain. Nevertheless, such profiles can be obtained statistically, and we have done this recently for most of the parameters that are related to auroral processes. We have also studied how the altitude profiles of the arc-associated parameters depend on Kp, ILAT, MLT, the solar illumination condition of the ionospheric footpoint and in the ion beam case also the solar cycle dependence. This presentation is a review and summary of the output of such statistical studies. For most parameters we will here, however, only show the seasonal and Kp effect on the altitude profile. To be able to easily compare results for the different parameters we choose to list them in each subsection. In section IV (Summary of observations) we take the results together.

A. Potential minima and their associated effective electric fields

In [20] we study how the altitude dependence of the mean energy, the potential minima and the effective electric field vary with different MLT, ILAT, Kp and seasonal conditions. The mapped-down effective ionospheric electric field is defined as the depth of the potential minimum divided by the mapped-down half-width of the structure in the ionospheric plane. The ionosphere is thus used as a reference altitude and the artificial effective electric fields are introduced just as a way to be able to compare electric fields measured at different altitudes.

In Figure 2, we show results for all data collected in the nightside MLT sectors for all Kp values during sunlit and darkness conditions. Panel (a) is the number of orbital crossings in each $0.5R_E$ radial bin. Panel (b) shows the depth (kV) of potential minima which are less than 0.6^o wide in ILAT (corresponding to 60 km in the ionosphere) and deeper than 0.5 kV. Panel (c) shows the effective ionospheric electric field $E_i > 100$ mV/m. Panel (d) is the occurrence frequency of $E_i > 100$ mV/m per orbital crossing, which is obtained by dividing the number of data points in panel c in each radial bin by the corresponding number of orbital crossings from panel a. The error bars correspond to $1/\sqrt{n}$ relative errors where n is the number of datapoints exceeding the threshold. Panel (e) is the occurrence frequency of $E_i > 500$ mV/m.

We summarise the results from Figure 2 as well as from Figures in [20]:

1) The potential minima (panel b Figure 2) found at low altitude are on the average more numerous and deeper than those found at high altitude.

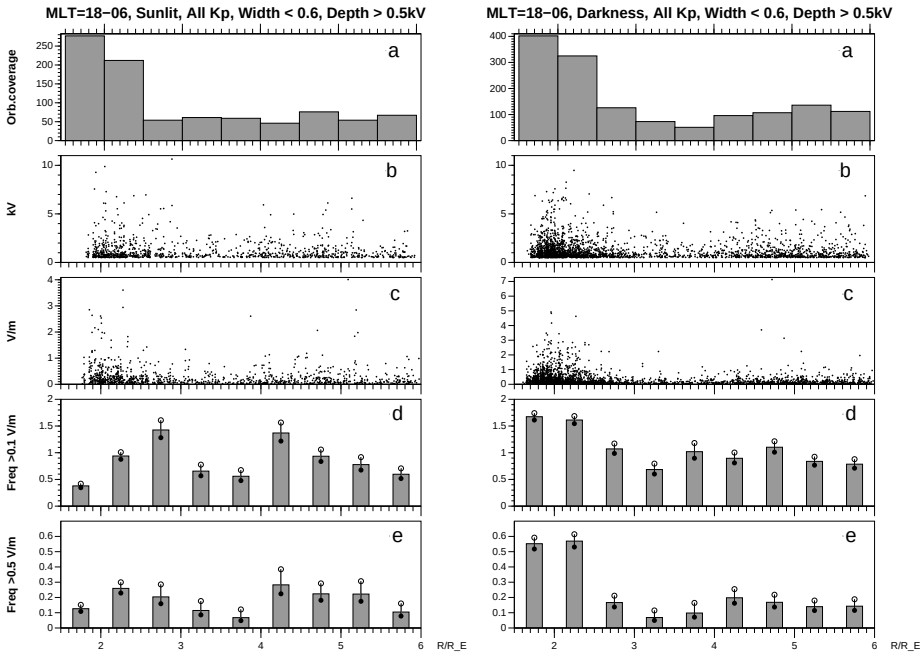

Fig. 2. All nightside potential minima deeper than 0.5 kV and the corresponding effective ionospheric electric fields E_i. The ILAT range is 65-74: (a) number of orbital crossings in each radial bin, (b) depth in kilovolts and radial distance of each potential minimum, (c) effective ionospheric electric field associated with each potential minimum with lower limit 100 mV/m, (d) occurrence frequency of E_i being larger than 100 mV/m (number of points in panel c divided by panel a), (e) occurrence frequency of E_i being larger than 500 mV/m.

2) The effective electric fields (panel c Figure 2) have higher values at low altitudes.
3) There is a dip in the occurrence frequency of the effective electric fields around 3.75 R_E radial distance (panel d and e Figure 2).
4) The high occurrence frequency of electric fields in the 4-6 R_E radial distance mainly comes from the midnight MLT (Figure 9 [20]). These high altitude electric fields might be substorm related. Thus in the other MLT sectors the electric fields almost exclusively occurs below about 3.75 R_E.
5) There is a peak in occurrence frequency of potential minima at about 2.75 R_E , however a seasonal and Kp dependence is also found which affects the peak altitude of the potential minima somewhat. For cases when the ionospheric footpoint is sunlit the maximum occurrence frequency is around $R = 2.75R_E$ while for cases of darkness conditions there is a downward shift of 0.5 R_E (panel d and e Figure 2).
6) Most potential minima occur in the dusk and midnight MLT sectors and their occurrence frequency increases with increasing Kp index (Figure 9 and 10 [20]).
7) When all nightside, Kp values and ionospheric illumination conditions are put together to form the baseline case, the maximum and minimum occurrence frequency of potential minima are found at $R = 2.25$ and 3.75 R_E (Figure 6, [20]).
8) The mentioned local minimum in the occurrence frequency of potential minima at about $R = 3.75$ is visible separately in all MLT sectors, all Kp and both sunlit and darkness ionospheres.

B. Upgoing ion beams

In [21] we study the occurrence frequency of upgoing ion beams as a function of altitude in different MLT sectors as well as invariant latitudes (ILAT), Kp, seasons and solar cycle conditions. To get the same altitude coverage (5000-30000km) as for the other parameters, we use two different ion instruments TIMAS and EICS from two satellites Polar and DE-1.

In Figure 3, we show results for all data collected in the nightside MLT sectors 18-06 for conditions where the satellite ionospheric footpoint is sunlit (left column) and in darkness (right column). The top panel of Figure 3 shows all ion beams between 0.5 and 10 keV as a function of radial distance R and beam peak energy. In the middle panels we show the number of hours spent by the instrument in each radial bin. By dividing the number of points in each bin by the number of samples coming from the bin we get the occurrence frequency of the ion beams in the bottom panels.

We summarise information from Figure 3 as well as from Figures in [21].

1) At low altitude ($R < 2.5R_E$) and high Kp, ion beams are mainly an evening sector phenomenon, while at high altitude ($R > 4R_E$) and low Kp they are more a midnight sector phenomenon (Figure 4 in [21]). This suggests that some high altitude ion beams in the midnight sector do not come from the ionosphere but

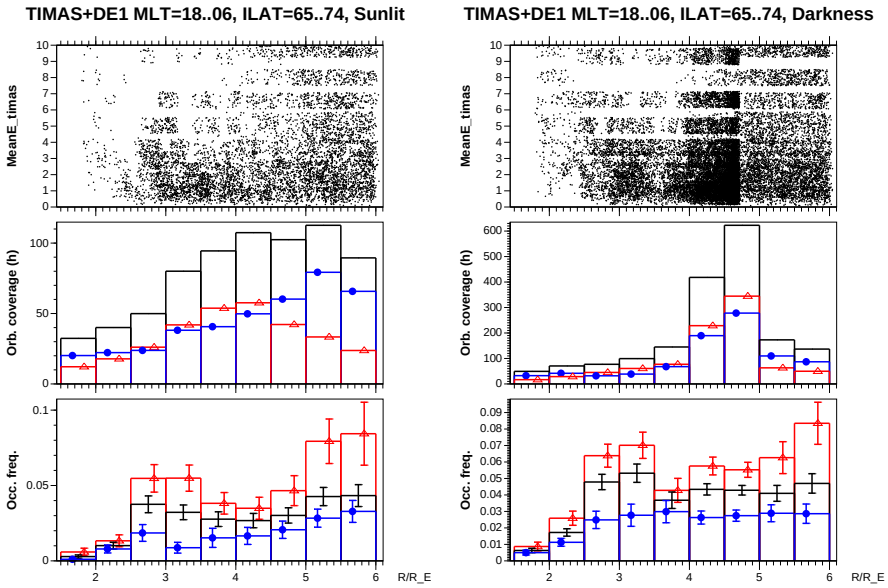

Fig. 3. Polar/TIMAS and DE-1/EICS ion beams in all the nightside MLT sectors as a function of radial distance R for sunlit (left column) and darkness conditions (right column). The ILAT range is 65-74. Top panel: Ion beam events (one event corresponds to 12 s sample) as function of radial distance and peak energy. Middle panel: Hours spent by the instrument in each radial bin. Bottom panel: Occurrence frequency of ion beams (number of points in each bin divided by the number of samples coming from the bin). Small Kp (≤ 2) shown by blue and filled circles, large Kp (> 2) by red and triangles. Black line is both Kp's put together.

originate as wave-particle interactions energising cold plasma at some intermediate altitude.

2) In the evening sector, a peak is also present in the invariant energy and particle fluxes carried by upward ion beams, where "invariant" means that both quantities are projected to the ionospheric plane (Figure 10 [21]).
3) Concerning ILAT, the peak is most visible in the 68-71 ILAT bin, probably because that corresponds to the average auroral oval latitude (Figure 6 in [21]).
4) The solar cycle does not have much influence on the ion beam occurrence frequency except through the Kp parameter (Figure 5 in [21]).
5) In the evening sector, a simple Monte Carlo simulation demonstrates that an O-shaped potential structure with some wave energisation can explain the altitude profile of the ion beam occurrence frequency, energy flux, particle flux and mean energy (Figure 10 in [21]).

C. Density depletions

Density depletions (auroral cavities) are studied in [23] by thresholding the Polar/EFI spacecraft potential during the years 1996-2000 (5000-30000 km altitude). The altitude dependence of the cavities is studied during varying conditions of MLT, ILAT, Kp and season. In this review we only show the Kp and seasonal conditions.

The density depletions are shown with three thresholds -11, -18, -25 V, the corresponding densities are 0.3, 0.1, 0.06 cm^{-3}.

In Figure 4 we show the occurrence frequencies of auroral cavities for the cases where the ionospheric footpoint is in darkness (left subplot) or sun-illuminated (right subplot). All nightside MLT (18-06) sectors are put together and the ILAT range is 65-74. The first panel shows the orbital coverage and the following panels show the occurrence frequency for the auroral cavities when three different spacecraft potential thresholds are used (-11 V, -18 V and -25 V) representing shallow, medium-deep and deep cavities, respectively. Small Kp index values ($0 \leq$ Kp ≤ 2) are shown by blue line with filled circles, large Kp index values (Kp > 2) by red line with open triangles, and all Kp's put together by black lines. We list the results below.

1) There is a peak in cavity occurrence frequency at about 3.25 R_E for darkness conditions and the region of cavities ends at about 4.25 R_E. In sunlit conditions the peak in occurrence frequencies is at 3.75 R_E and the region of cavities extends up to 5.25 R_E (Figure 4).
2) The peak in occurrence frequencies of auroral cavities is clearest for deepest cavities, corresponding to plasma densities smaller than $\sim$ 0.6 cm^{-3} (Figure 4).
3) The Kp index does not have a clear effect on the peak altitude (Figure 4).
4) For low ILAT, cavities occur mainly only for large Kp, probably because the auroral oval extends equatorward during disturbed conditions. For other ILAT, however, cavities are more common for low Kp than for high Kp (Figure 5 and 6 [23]).
5) Cavities show an auroral zone dependency, which indicates that most of them are associated with auroral processes (Figure 3 [23]).
6) In the midnight sector there are cavities also in the 4-6 R_E radial distance range for both low and high Kp.

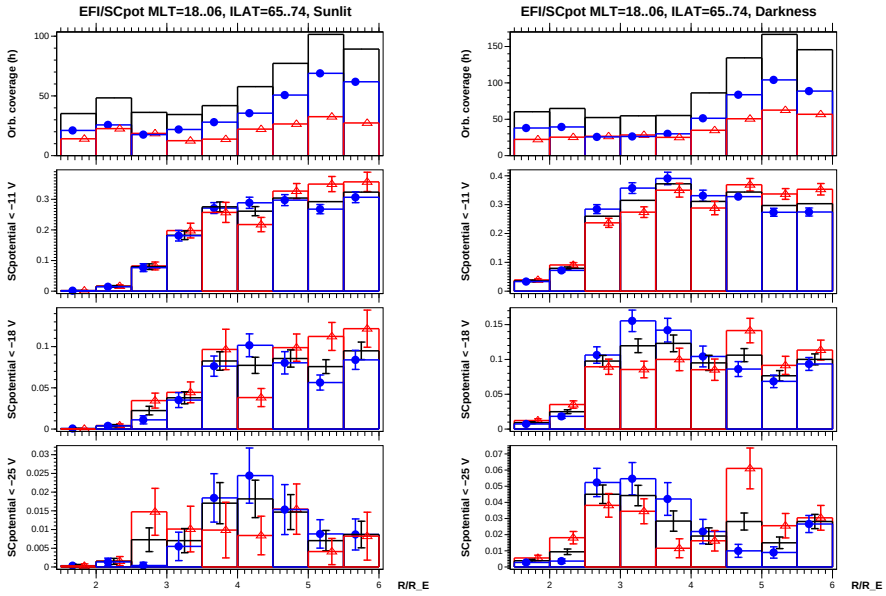

Fig. 4. Occurrence frequency of nightside auroral cavities for radial distances between 1.5 to 6 R_E. Left subplot show the occurrence frequencies for conditions when the ionospheric footpoint is in darkness and the right subplot for sun-illuminated conditions. Top panels: the orbital coverage in hours. Panels 2-4: the occurrence frequency for spacecraft potential thresholds -11 V, -18 V and -25 V. All Kp's put together is shown by a black line. Low Kp (≤ 2) is shown by blue lines with filled dots and high Kp (> 2) by red lines and open triangles. Error bars are also shown.

They also occur in the morning sector, but only for high Kp. This holds for ILAT range 68-74. These cavities may be related to substorms (Figure 5 and 6 [23]).

D. Electrostatic wave bursts

In [31] we study the occurrence frequency of the 1-10 Hz electric wave component in the auroral zone (65-74 ILAT) using observations from the Polar/EFI instrument. We investigate the altitude dependence of the occurrence frequency during varying Kp, MLT, ILAT and seasonal conditions. We especially discuss waves with significant parallel component ($E_\parallel < 0.4E_\perp$ and $E_\perp \geq 1$ mV/m). In this review we only show the seasonal and Kp dependence (see Figure 5).

In Figure 5 we investigate the occurrence frequency of parallel-dominated waves decomposed into sunlit and darkness conditions respectively. In the first panel the orbital coverage in hours is shown and in the bottom panel the occurrence frequency for the parallel dominated waves is seen for the radial distances 1.5-6 R_E. Red lines correspond to conditions where Kp > 2 and blue lines represent $0 \leq$ Kp ≤ 2. Black lines correspond to cases when all Kp's are put together. We list the results seen in Figure 5.

1) The preferred radial distance of parallel-dominated waves is 3.25 R_E when the ionospheric footpoint of the satellite is in sunlight, but moves to 2.75 R_E when it is in darkness (Figure 5).
2) The occurrence frequency of parallel-dominated waves is usually larger for high Kp than for low Kp index (Figure 5).
3) Constant occurrence frequency contours of the parallel-dominated waves qualitatively follow the average auroral oval (in the ILAT-MLT plane), (Figure 7, [31]).
4) The occurrence frequency of perpendicular-dominated waves decreases smoothly with altitude (Figure 4, right subplot, [31]).

E. Anisotropy

Often the electron distribution in auroral field lines consists of at least two quasi-Maxwellian populations, each with possibly different parallel and perpendicular temperatures $T_\parallel$ and $T_\perp$. Especially cases where the hot population is isotropic but the cold populations has $T_\parallel > T_\perp$ asymmetry are common and are studied in [22].

The anisotropy of electrons is studied with the Polar/HYDRA instrument during the years 1996-2000 (5000-30000 km altitude). The altitude dependence of especially the middle-energy electrons (100-1000 keV) is studied with varying MLT, ILAT and Kp.

In Figures 6 and 7 show the basic statistical results of $T_\parallel > T_\perp$ middle-energy (100-1000 eV) electron anisotropies. The major findings are as follows.

1) The middle-energy anisotropies (100-1000 eV) obey the MLT-ILAT dependence of the average auroral oval. The distributions of the low and high-energy anisotropies are more irregular (Figure 6).
2) The altitude profile of the anisotropies is smooth as one would expect since electrons have high mobility along the magnetic field (Figure 7).
3) There is often an isotropic electron distribution at higher energies simultaneously with the anisotropy (Figure 2 and 4 [22]).

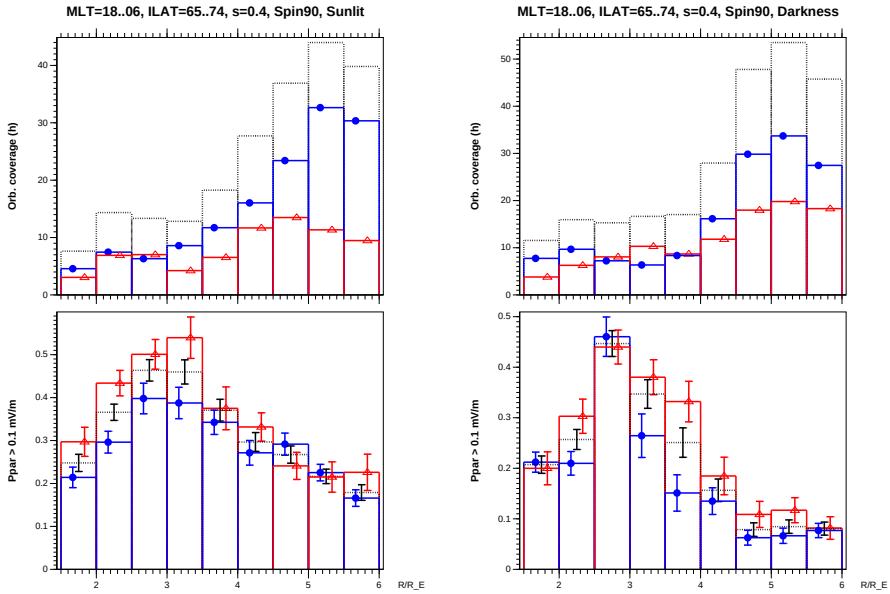

Fig. 5. The occurrence frequency of the parallel dominated waves during conditions when the satellite footpoint is sunlit (left subplot) and conditions of darkness (right subplot). All nightside MLT sectors are put together and the ILAT range is 65-74. On the horizontal axis the radial distance between 1.5-6 R_E is shown. Top panel: the orbital coverage in hours. Bottom panel: the occurrence frequency for the parallel dominated waves ($E_{||} < 0.4E_{\perp}$ and $E_{\perp} \geq 1$ mV/m). Blue line with filled circles corresponds to low Kp ($0 \leq$ Kp ≤ 2, red line with triangles is for high Kp (Kp > 2) and when all Kp's are put together it is represented with a black line.

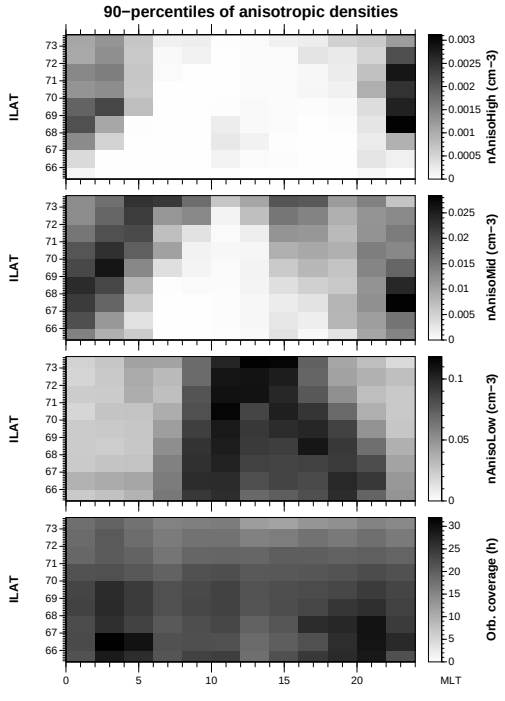

Fig. 6. Strength of $T_{||} > T_{\perp}$ electron anisotropies in different energy ranges: 10-100 eV (top), 100-1000 eV (second panel), 1-10 keV (third panel) and orbital coverage (bottom) as a function of MLT and ILAT. Especially the middle-energy anisotropies (100-1000 eV, second panel) follow the pattern of the average auroral oval.

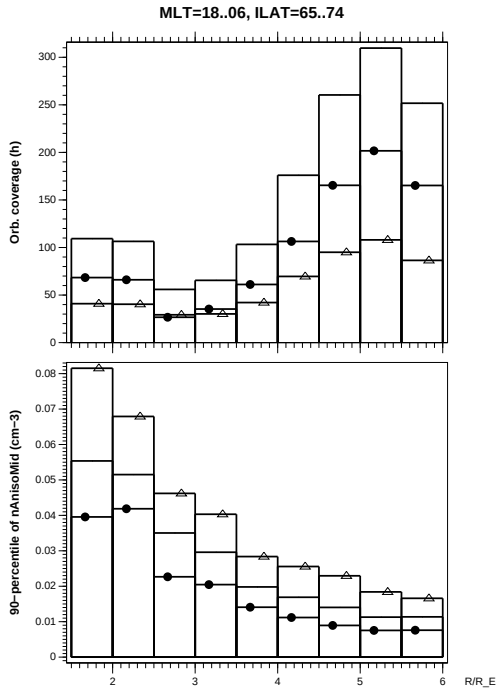

Fig. 7. Top: orbital coverage. Bottom: Strength of middle-energy (100-1000 eV) electron anisotropies as function of radial distance in the nightside. Dots show low Kp (≤ 2) and triangles high Kp (> 2), black line all Kp.

4) The anisotropies are often up/down symmetric (Figure 2 and 4 [22]).
5) The middle-energy anisotropies appear at lower ILAT in all MLT sectors when the Kp index increases as is expected for an auroral oval related process (Figure 8 [22]).

F. Ion shells

By ion shell we mean a 3-D spherical almost hollow shell in velocity space. Such distributions can be formed by a variety of mechanisms, including various time of flight effects and energy-dependent perpendicular ion drifts, and they potentially contain a lot of free energy. An example of a half-consumed ion shell is given in Figure 8, where also the simultaneously occurring electron middle-energy anisotropy is shown (right subplot). Our interpretation is that below the spacecraft, part of the free energy has gone to waves that have energised the electrons, so that only the downgoing part is a pure ion shell.

Statistically, in Polar data ion shell distributions occur either close to the polar cap boundary or at low latitudes (Figure 9 left subplot). The low latitude ones are the most common. In the radial direction, there is some preference for ion shells to occur at 3-4 R_E radial distance, although quantitative conclusions cannot be drawn because of incomplete orbital coverage (Figure 9, right subplot).

Ion shells occur less frequently in the auroral zone than around it (Figure 9 left subplot, white area in middle and bottom panels). There are two possible explanations: (1) the mechanisms producing the shell does not operate in the auroral zone, (2) the mechanisms operate also there, but the auroral zone shells are quickly consumed by wave-particle interactions and thus eroded away. To find out which is the more correct explanation one would need ion shell distribution data at higher altitude.

IV. Summary of observations

We review the latest results on the altitude dependence of auroral potential structures, upgoing ion beams, density depletions, electron middle-energy anisotropies($\sim$50-500 eV), electrostatic wave bursts and ion shell distributions. These parameters are all probably related to the auroral electron acceleration process and thus finding out their altitude dependence gives valuable information about auroral acceleration. We have also discussed how the altitude profiles of the mentioned parameters depend on Kp, ILAT, MLT and the solar illumination condition of the ionospheric footpoint.

Below we list the major results from the studies.

1) In all parameters (potential structures, upgoing ion beams, cavities and waves with a large parallel component) there is peak in occurrence frequency at $\sim$ 3 R_E radial distance.
2) Peak amplitude and altitude depend on solar illumination condition (season), Kp index, ILAT and MLT, in the same way for potential structures, ion beams, cavities and waves.
3) Increase in occurrence of potential structures and cavities above $R = 4R_E$ takes place in midnight MLT sector (22-02). This is likely due to some midnight-specific high altitude process which is different from ordinary auroral arcs; it may be related to substorms.
4) Increase in occurrence frequency of ion beams above $R = 4R_E$ takes place probably due to wave heating. This is a process which is peculiar to ion beams and thus it has no counterpart in the other parameters.
5) There is indirect event-based and simulation evidence that Bernstein waves driven unstable by ion shell distributions energise the electrons in the parallel directions, thus forming $T_\parallel > T_\perp$ electron anisotropies.

V. Simulations

We use 2-D electrostatic hybrid and kinetic simulations to model the development of auroral potential structures. The hybrid code shows how a potential structure arises from wave-particle interactions, and the kinetic simulation shows a possibility how such waves may be formed: free energy associated with a hot ion shell distribution.

A. Electrostatic hybrid simulation

The 2-D hybrid simulation code of [19] has particle ions and quasineutral fluid electrons obeying the Boltzmann response. It employs a new type of ion pusher ("monopole solver") which makes it possible to use timesteps as long as $v_i/\Delta x_\parallel$ instead of the usual $v_i/\Delta x_\perp$, where v_i is the maximum ion velocity and $\Delta x_{\parallel,\perp}$ is the grid spacing in the parallel and perpendicular directions, respectively. The simulation box is aligned with the dipole magnetic field and is 20 km wide in the ionosphere and 38000 km long along the magnetic field. The energy source is provided by wave-particle interactions with the electrons. The waves are assumed to be localised in ILAT and thus define the boundaries of the auroral arc that forms.

Figure 10 shows the ionospheric ion density and the potential in the hybrid simulation after the wave-particle interactions have been on for 10 minutes. A density cavity, upgoing ion beam and a closed potential structure have formed.

We summarise the main results from the hybrid simulation:

1) With wave-particle interactions turned on, the simulation produces a self-consistent O-shaped potential structure (Figure 10, right subplot) with an associated density cavity (Figure 10, left subplot). If a shear flow topside boundary condition is used without wave-particle interactions, a U-shaped potential is produced.
2) Strong convergent perpendicular electric fields are confined in a relatively narrow altitude range (about 5000-11000 km, Figure 7 [19]).
3) Upward electric fields of about 1 mV/m exist at the bottom of the potential structure, while at higher altitude there are weaker downward fields (Figure 8 [19]).
4) When the driver is turned off, the potential structure disappears in the electron time scale ($\sim$ 1 s) and the density depletion in the ion time scale ($\sim$10 min) (Figure 9 [19]).
5) The arc becomes stronger if the anisotropy is increased. The potential structure bottom altitude becomes lower if the ionospheric source plasma density is decreased (Tables 1 and 2 [19]).

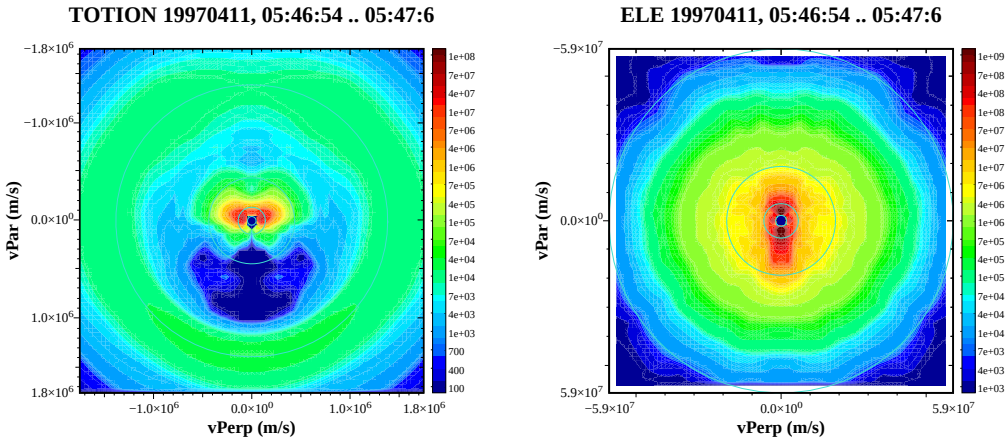

Fig. 8. Left subplot: Ion shell distribution in Polar/TIMAS data (green circular area). Upgoing low energy ion shell is also seen (yellow and red). Right subplot: Simultaneous electron distribution, where middle-energy $T_{||} > T_{\perp}$ anisotropy is seen.

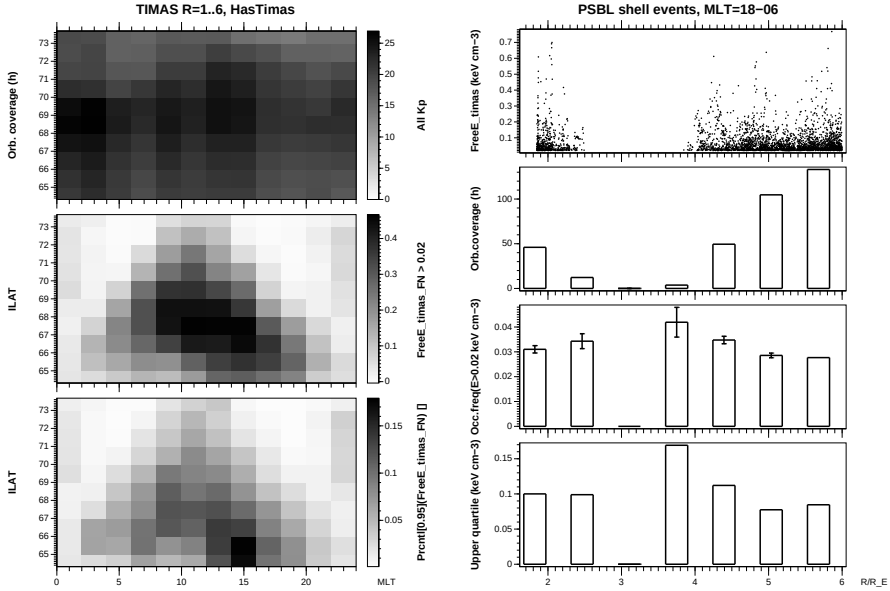

Fig. 9. Left subplot: Ion shells as function of MLT and ILAT. Orbital coverage (top), occurrence frequency of ion shells obtained by thresholding (middle) and their 95-percentile (bottom). Right subplot: Ion shells as function of radial distance. Detected ion shell free energy densities (top), orbital coverage (second panel), occurrence frequency obtained by thresholding (third panel) and upper quartile (bottom).

B. 2-D electrostatic PIC simulation

The 2-D electrostatic kinetic simulation is a conventional explicit particle-in-cell code with realistic electron mass [24]. The box size parallel and perpendicular to the magnetic field is 800 and 10 km, respectively (Figure 11). Initially there is free energy in the plasma in the form of a hot ion shell distribution. The free energy drives unstable ion Bernstein waves. The main results are:

1) A hot ion shell distribution may contain enough free energy to power the aurora (Figure 2 panel j [24]).
2) Ion shell distributions do occur on auroral field lines. We have found cases where the data are clearly consistent with the assumption that the shell distribution provides the free energy for wave-induced parallel electron energisation (Figure 2 [24]).
3) The perpendicular e-folding distance of the ion Bernstein waves in question is of the order of the auroral arc width (a few kilometres) or smaller when projected to the ionosphere (Table 1 [24]). The parallel e-folding distance is a few hundred kilometres, which is smaller than the field-aligned extent of the energisation region. These properties of the Bernstein waves are consistent with the physical size of the region where they exist.
4) Electrons are heated in the parallel direction by the Bernstein waves at a rate $\sim$ 80 eV/s (Figure 13 [24]).

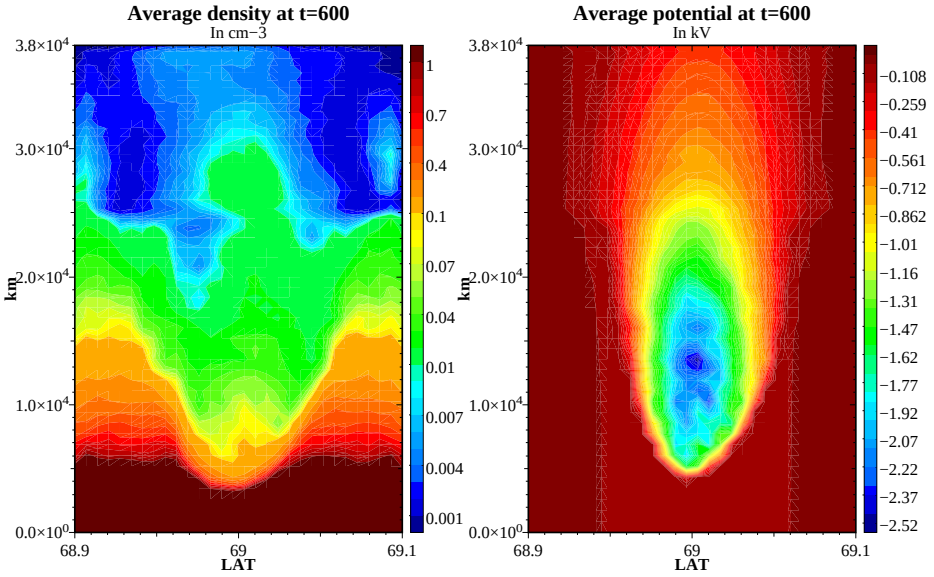

Fig. 10. Left subplot: density of ionospheric ions after auroral arc has formed in the hybrid simulation. Horizontal axis is ILAT and vertical is altitude measured along dipolar magnetic field. Right subplot: corresponding potential structure, with maximum depth 2.52 kV.

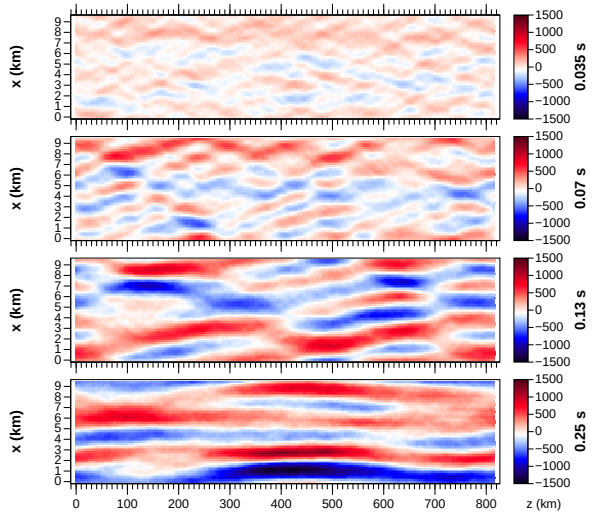

Fig. 11. Time development of Bernstein wave electric potential in the kinetic simulation. Horizontal axis is along magnetic field (box length 800 km) and vertical axis is perpendicular (box width 10 km). From top to bottom the times are 5, 70, 130 and 250 ms. The maximum wave amplitude is 1.5 kV.

Cold ions receive only 10% of the heating (their heating is perpendicular).

5) An inverse cascade process for the Bernstein waves is in operation which transfers energy from short to long wavelengths by nonlinear mechanisms (Figure 11).

VI. Theory and a small simulation

The observations reviewed above give rise to important consequences concerning the physics of auroral electron acceleration. Exactly what these consequences are is not quite straightforward. We now present the model which we have arrived at studying the data and which we find also theoretically pleasing. Afterwards we discuss to what extent the model is unique, i.e. could our observations be explained by other models.

A. The Cooperative Model

A central concept in the model is a closed (O-shaped) negative potential structure. The structure is formed by the following steps:

1) Broadband plasma waves (maybe ion Bernstein modes, [24]) get unstable by a presence of some free energy source. The free energy is probably in the hot ion distribution, possibly in the form of an ion shell distribution [24].
2) The waves energise electrons in parallel and to a lesser extent ions in perpendicular direction. In case of ion Bernstein waves driven unstable by an ion shell distribution, the particle-in-cell simulation produced the rate of energisation 80 eV/s [24]. The result is an anisotropic ($T_{\|} > T_{\perp}$) electron distribution [16], [22]. If the electron energisation comes from Landau resonance, the anisotropy may be limited in energy [22].
3) The electron anisotropy causes the electron mirror points to move downward since the pitch angles decrease. Since the flux tube becomes narrower at lower altitude, the number of electrons per volume tends to increase. As the ions do not act similarly, the result is a tendency to form a negative charge cloud whose density increases downward.
4) Since the electron Debye length is only $\sim$ 100 m, quasineutrality must be maintained. Thus the charge cloud never actually forms, but a downward electric field is set up which restores quasineutrality. This happens so fast that ions do not have time to react.

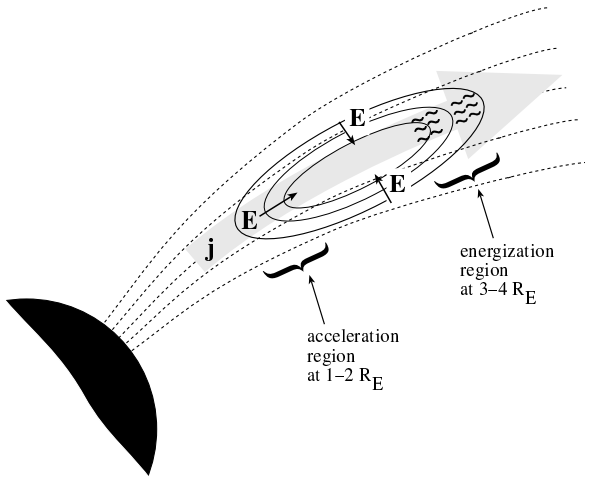

Fig. 12. Sketch of our proposed model for auroral acceleration. With the help of wave-particle interactions, electrons are energised in the parallel directions and are thus able to climb the potential hill in the energisation region. Thereafter they undergo electrostatic acceleration, which produces peaked energy spectra at low altitude. The engine is the wave-particle interaction, while the "gears and wheels" (geometry and transfer between kinetic and potential energy) is provided by the potential structure. The potential structure is formed by space charges produced by the wave-particle interactions and mirror force. The system is maintained self-consistently as long as there is free energy for the waves to consume.

5) The ionosphere and magnetosphere are maintained in approximately zero potential. Thus the potential contours must close by forming a closed potential structure. Another way to see this is to note that parallel electric field cannot exist in plasma which contains cold electrons, and at low enough altitude cold electrons of ionospheric origin always exist.

Once the O-shaped potential structure has formed with the help of waves and anisotropies [22], it gives rise to a number of additional observational consequences:

1) Strong perpendicular electric fields are confined to the altitude where the potential structure exists [20].
2) Since the bottom of the structure contains an upward parallel electric field, inverted-V electron spectra are produced at low altitude [15].
3) Upgoing ion beams gain energy at the bottom of the potential structure and lose it again in the upper part of it [21].
4) O-shaped potential structure is a density depletion: it repels electrons, and ions speed up inside it [23]. Thus the structure remains stable [19].
5) 1-10 Hz plasma waves with significant parallel component exist at the same altitude where the topside of the potential structure probably resides [31]. The waves might be another byproduct of the potential structure, e.g. ion acoustic waves generated by rapid movements of the potential structure. The exact nature of the parallel-dominated waves has not been confirmed yet, however.

The energy flows through the system in the following way:

1) Ion shell distribution gives energy to plasma waves [24].
2) Plasma waves energise electrons in parallel direction, and as a byproduct they also contribute to perpendicular ion heating [24].
3) When energising the electrons, the waves must work against the downward electric field in the energisation region (Figure 12). This means that the energy extracted from the waves is soon translated from kinetic to potential energy. In case of Landau resonance, this may help keep the electrons in the resonant velocity range for a longer than would be the case without the downward electric field. Thus the presence of the downward field may increase the total power that is extracted from the waves [15].
4) When an electron reaches the centre of the potential structure, it experiences a "free fall" acceleration towards the ionosphere exactly as in the traditional U-potential model. This releases its potential energy and turns it into kinetic energy. The observational manifestation is the appearance of inverted-V electron spectra at low altitude. The auroral electron beams have many secondary phenomena associated with them below the acceleration region (optical auroral arcs, secondary wave-particle interactions, etc.).

We call the model as a whole the "Cooperative Model" (CM), because in it, the plasma waves and the potential structure both contribute to electron acceleration in an essential way. One characterisation of the CM is that the plasma waves are the engine and the potential structure is the "gears and wheels". The energy is provided by the plasma waves, but many of the important observational characteristics would not exist without the potential structure. Indeed, it is meaningless to ask how electron acceleration would look like without a potential structure, since the emergence of the potential structure is an inescapable consequence of the action of the waves.

B. Is Cooperative Model unique?

Although we have pointed out above that many aspects of the CM are in accordance with observations and that the model is also compatible with test particle and plasma simulations, one can ask if the observations could be explained by other models:

1) The observation that strong perpendicular electric fields are confined below $\sim 4R_E$ radial distance (Figure 3 [20]) could perhaps also be explained by a widening of a U-shaped potential structure as in the potential finger model of [28].
2) The fact that auroral density depletions also have a preferred altitude range (Figure 4) could be explained if there is another layer of upward electric fields at high altitude [9]. The auroral cavity would then be sandwiched between two layers of upward fields.
3) The electron anisotropies [22] could correspond to ionospheric return current regions (upward beams) instead of being produced in the magnetosphere [25]. The fact that the anisotropies are often up-down symmetric might be due to insufficient instrument time resolution or by

symmetric return current regions working in the opposite hemisphere.

4) The fact that ion beams have a dip at $\sim 4R_E$ radial distance (Figure 3) is hard to explain in the U-potential model, i.e. without downward electric fields.

Thus it seems in principle possible to explain the behaviour of all mentioned parameters except the ion beam behaviour without necessarily invoking a closed potential structure. How compatible these alternative explanations would be with low-altitude observations is another matter. For example, if a U-shaped potential structure widens, the corresponding low-altitude inverted-V regions should also be wide, not narrow, since the electrons undergo potential drop acceleration regardless of the altitude of the potential drop. The multitude of perpendicular scale sizes present in the auroral arcs may leave room for both types of models [30]. If it is so, then the O-shaped model probably corresponds to narrow auroral arcs (few kilometre width in the ionosphere). We remark that a closure of the potential before the opposite hemisphere (which in our terminology is an O-shaped potential) was independently suggested by *Hallinan and Stenbaek-Nielsen* [12] from studying the degree of conjugacy of auroral arcs in the two hemispheres.

C. How anisotropy produces potential structure

We now come back to item 3 in subsection VI.A (The Cooperative Model) above, i.e. the question how a $T_\parallel > T_\perp$ electron anisotropy produces a downward electric field. Consider a bi-Maxwellian equatorial plane distribution function $f_0(v_\parallel, v_\perp)$,

$$f_0(v_\parallel, v_\perp) = \frac{n_0}{T_\perp \sqrt{T_\parallel}} \left(\frac{m}{2\pi}\right)^{3/2} \exp\left(-\frac{mv_\parallel^2}{2T_\parallel} - \frac{mv_\perp^2}{2T_\perp}\right) \quad (1)$$

where m is the electron mass, n_0 the electron density and $T_\parallel$, $T_\perp$ the parallel and perpendicular temperatures in energy units, respectively. At other points on the field line, Liouville's theorem states that $f(v_\parallel, v_\perp) = f_0(v_\parallel^0, v_\perp^0)$ where $v_\parallel^0$,$v_\perp^0$ are the equatorial plane values of the particle velocity. The connection between $v_\parallel$,$v_\perp$ and $v_\parallel^0$,$v_\perp^0$ can be worked out from the conservation of total energy $E = (1/2)m(v_\parallel^2 + v_\perp^2) + qV$ and the magnetic moment $\mu = (1/2)mv_\perp^2/B$. The electron density at point s ($s = 0$ corresponds to equatorial plane) is given by

$$n(s) = 2\pi \int_{-\infty}^{\infty} dv_\parallel \int_0^{\infty} dv_\perp v_\perp f(v_\parallel, v_\perp) \quad (2)$$

which gives after doing the integrations

$$n(s) = \frac{n_0 \exp\left(-qV(s)/T_\parallel\right)}{\frac{T_\perp}{T_\parallel}\left(1 - \frac{B_0}{B}\right) + \frac{B_0}{B}} \quad (3)$$

where B_0 is the equatorial plane magnetic field. Often a useful approximation is $B_0 \approx 0$ in which case we obtain

$$n(s) = \frac{T_\parallel}{T_\perp} n_0 \exp\left(-qV(s)/T_\parallel\right). \quad (4)$$

All particle populations obey a similar relation. The quasineutrality gives the equation $n_e^{\rm tot} = n_i^{\rm tot}$ which binds together different populations. If there is only one ion and one electron population, this equation can be solved analytically, which yields

$$eV(s) = \frac{T_e^\parallel T_i^\parallel}{T_e^\parallel + T_i^\parallel} \log\left(\frac{T_e^\perp T_i^\parallel}{T_e^\parallel T_i^\perp}\right) \quad (5)$$

in the limit $B_0 \to 0$. Alfvén and Fälthammar [2] considered a similar problem, but as they used delta function populations instead of Maxwellians, their formulas are not directly comparable to ours. If ions are isotropic ($T_i^\parallel = T_i^\perp \equiv T_i$) and $T_i \ll T_e^\parallel, T_e^\perp$, we obtain

$$eV(s) = -T_e^\parallel \log\left(\frac{T_e^\parallel}{T_e^\perp}\right) \quad (6)$$

which gives the magnitude of the negative potential that arises from a cigar-shaped ($T_e^\parallel > T_e^\perp$) electron anisotropy far away from the equatorial plane. In case of multiple ion and electron populations while still using $B_0 \to 0$ the equation from which $V(s)$ must be numerically solved reads

$$\sum_e \alpha_e n_e \exp(eV/T_e^\parallel) = \sum_i \alpha_i n_i \exp(-eV/T_i^\parallel) \quad (7)$$

where $\alpha = T_\parallel/T_\perp$ is the temperature anisotropy of each population and n_i is the partial density of the population in the equatorial plane. When Eq. (7) is solved with an anisotropic population present (one of the α's is larger than unity), V must be adjusted so that the equation is satisfied. The solution V will be of the order of $T^\parallel$ of the coldest population whose partial density n exceeds $(\alpha - 1)n$ of the anisotropic component. Thus, if cold electrons are present, the potential is small as long as the anisotropy is below some threshold which depends on the partial densities and becomes large if the threshold is exceeded (see also Eqs. 9 and 10 in reference [19]).

All the formulas of this subsection ignore the nonlinear feedback between the potential structure and the electrons, since they assume that the electron distribution is not affected by the potential. Therefore only potentials which are of the same order as the parallel temperature of the electrons can be produced. According to low-altitude satellite observations, however, the potential is often ~ 3 times larger than the thermal energy [29], [30]. We shall now deal with a possible theoretical explanation.

D. Simple 1-D PIC simulation

Thus far we have simulated the global formation of the O-shaped potential structure when a primary charge cloud (more accurately: a tendency to form such a cloud) is put in by hand [19], and on the other hand the wave-particle interaction between ion Bernstein waves and electrons has been directly simulated [24]. What is still missing is a combination of the two, i.e. a particle-in-cell simulation with so large simulation box that the whole potential structure fits in it. While waiting for the computing power necessary to perform such a calculation to become available, we present here a one-dimensional electrostatic particle-in-cell simulation. The basic characteristics of the simulation are as follows. The ion dynamics is ignored, thus the ions form a stationary

TABLE I
POTENTIAL DROP DEPENDENCE ON STRENGTH OF WAVE-PARTICLE INTERACTION ω. STRENGTH OF AVERAGE AND MAXIMUM DOWNWARD ELECTRIC FIELD IS ALSO GIVEN.

ω (s^{-1})	Potential drop (V)	Average E (mV/m)	Maximum E
0.5	620	0.03	0.08
1.0	1380	0.07	0.22
1.5	2100	0.1	0.21
2.0	2700	0.135	0.32

background charge density. The equations to be solved are the adiabatic electron equation of motion containing the mirror force and the electric force terms, and Poisson's equation. Implicit time integration is used to reduce unwanted oscillations at the plasma frequency [4]. The density is artificially reduced (electron Debye length enlarged) to make the simulation run quickly. 200 grid cells and 300 electrons per cell are used with quadratic spline weighting [4]. The magnetic field has a dipolar $1/r^3$ dependence. The Poisson equation is written as

$$-\nabla^2\Phi = -\frac{1}{r^3}\frac{\partial}{\partial r}\left(r^3\frac{\partial\Phi}{\partial r}\right) = \frac{e(n_i - n_e)}{\epsilon_0}, \qquad (8)$$

which we justify by analogy with the spherical case (magnetic monopole case) where the Laplacian would be $\nabla^2 = (1/r^2)(\partial/\partial r)(r^2(\partial/\partial r))$. Notice that argument cannot be made rigorous as the dipole geometry is symmetric with respect to only one coordinate (the longitude angle). However, we have run the program both using the monopole and dipole fields and the results are qualitatively very similar. Since the dipole case is easier to compare with observations, we use it in the following. The radial distance range of the simulation box is 2-5.1 R_E ($2\cdot10^7$ m). The initial electron temperature is 300 eV in both parallel and perpendicular directions. Particles are mirrored at the bottom boundary, i.e. ionospheric losses are ignored. When an electron reaches the top boundary its parallel velocity is re-randomised and drawn from 300 eV Maxwellian distribution. This corresponds to neglecting the effect of the opposite hemisphere, which is justified if a large volume of the flux tube exists above the top boundary.

The wave-particle interactions are added to the simulation as follows. At each timestep, if the parallel energy of an electron is in the range 100-1000 eV, its parallel velocity is multiplied by $(1 + \omega\Delta t)$, where Δt is the timestep (30 ms). Here ω is a parameter controlling the strength of the wave-particle interactions.

Table 1 shows the potential drop dependence on ω. In each case the simulation is run for 30 s and the potential drop is determined from the time-averaged electric field. The potential depends roughly linearly on r so that the time-averaged downward electric field E is roughly constant. The average and maximum E is also given in Table 1. For large ω, fluctuations during the run become stronger. The fluctuations are slowly reduced if the number of particles per cell is increased. We verified that the results presented in the table do not change much if 3000 particles per cell are used instead of 300.

Although this simulation lacks many important features, it illustrates how a downward electric field can form because of wave-particle interactions and that depending on the strength of the wave-particle interactions, the strength of the associated potential drop can much exceed 300 eV, which is the original electron thermal energy. This nonlinear effect occurs because the downward electric field enables electrons to stay in the resonant velocity range for a longer time than what would be otherwise possible, which increases the total power drawn from the waves. If one varies the parameters (e.g. the resonant energy range), the resulting numbers differ, but the behaviour remains similar.

VII. CONCLUSIONS

Using statistical analysis of electric field, ion, electron and wave data from Polar satellite together with different types of simulations, we have shown that the data and simulations are consistent with a picture of auroral acceleration that we call the Cooperative Model. The model describes the shape of the electric field structure and how energy is transferred in several steps from the hot ion distribution finally to auroral electrons. The model does not yet explain the horizontal scale of auroral arcs or their multiplicity. Explaining these observational characteristics must wait for a more detailed study of the hot ion distribution free energy source and how that is formed deeper in the magnetosphere. Also the return current region is not yet a self-consistent part of the model: what is missing is the mechanism for generating perpendicular electric currents in the magnetosphere. Finally, the role of Alfvén waves is still unclear. It has been widely known for decades that Alfvén waves exist and probably play some role in auroral electron energisation, but their relationship to the potential structure acceleration has not yet been studied much. Our guess is that Alfvénic power is responsible for the energy needed in deforming auroral arcs and maybe also for the associated ionospheric Joule heating, but that the electrons forming the arcs are mostly energised by the processes described in this paper.

While we have found statistical studies very useful, to finally judge what is the instantaneous shape of the potential structure one would need magnetic conjunctions of at least three satellites in different altitudes below, within and above the potential structure. The occurrence frequency of three-satellite conjunctions is currently almost zero. To obtain such conjunctions, a specifically designed multi-satellite mission is required. Having three or more satellites in circular orbits whose periods are related to each other as small integers would be ideal. Furthermore, choosing the orbit periods to be integer fractions of the sidereal day would allow a ground-based observation of each conjunction, which would increase the benefits of such a mission even more.

ACKNOWLEDGEMENT

The authors would like to thank W.K. Peterson, F.S. Mozer, C.A. Kletzing and C.T. Russell for providing the Polar TIMAS, EFI, HYDRA and MFE data, respectively. They are also grateful to Harri Laakso, Andris Vaivads and Mats André for useful discussions. We thank Hannu Koskinen for reading the manuscript and giving a number of comments. The work

of AO was supported by the Swedish Research Council and that of PJ by the Academy of Finland.

REFERENCES

[1] Alfvén, H., On the theory of magnetic storms and aurora, *Tellus*, 10, 104, 1958.

[2] Alfvén, H. and C.-G. Fälthammar, Cosmical electrodynamics, Clarendon, Oxford, 1963.

[3] Bingham, R., D.A. Bryant and D.S. Hall, Auroral electron acceleration by lower-hybrid waves, *Ann. Geophys., 6,* 159-168, 1988.

[4] Birdsall, C.K. and A.B. Langdon, Plasma physics via computer simulation, McGraw-Hill Book Company, Singapore, 1985.

[5] Block, L.P., Potential double layers in the ionosphere, *Cosmic Electrodynamics*, 3, 349, 1972.

[6] Bryant, D.A., A.C. Cook, Z.-S. Wang, U. De Angelis and C.H. Perry, Turbulent acceleration of auroral electrons, *J. Geophys. Res., 96*, 13829–13839, 1991.

[7] Bryant, D.A., *Electron acceleration in the aurora and beyond* (Institute of Physics Publishing, Bristol 1999).

[8] Carlqvist, P. and R. Boström, Space-charge regions above the aurora, *J. Geophys. Res., 75*, 7140–7146, 1970.

[9] Ergun, R.E., C.W. Carlson, J.P. McFadden, F.S. Mozer and R.J. Strangeway, Parallel electric fields in discrete arcs, *Geophys. Res. Lett., 27,* 4053–4056, 2000.

[10] Frank, L.A. and K.L. Ackerson, Observations of charge particle precipitation into the auroral zone, *J. Geophys. Res., 76*, 3612-3642, 1971.

[11] Gurnett, D.A. and L.A. Frank, Observed relationship between electric field and auroral particle precipitation, *J. Geophys. Res., 78*, 145-170, 1973.

[12] Hallinan, T.J. and H.C. Stenbaek-Nielsen, The connection between auroral acceleration and auroral morphology, *Phys. Chem. Earth*, 1–3, 26, 169–177, 2001.

[13] Harvey, P., F.S. Mozer, D. Pankow, J. Wygant, N.C. Maynard, H. Singer, W. Sullivan, P.B. Anderson, R. Pfaff, T. Aggson, A. Pedersen, C.G. Falthammar and P. Tanskanen, The electric field instrument on the polar satellite, Space Science Reviews 71, 583-596, 1995.

[14] Janhunen, P., A. Olsson, F.S. Mozer and H. Laakso, How does the U-shaped potential close above the acceleration region? A study using Polar data, *Ann. Geophys., 17*, 1276–1283, 1999.

[15] Janhunen, P. and A. Olsson, New model for auroral acceleration: O-shaped potential structure cooperating with waves, *Ann. Geophysicae,* 18, 596–607, 2000.

[16] Janhunen, P., A. Olsson, W.K. Peterson, H. Laakso, J.S. Pickett, T.I. Pulkkinen and C.T. Russell, A study of inverted-V auroral acceleration mechanisms using Polar/Fast Auroral Snapshot conjunctions, *J. Geophys. Res., 106*, 18995–19011, 2001.

[17] Janhunen, P. and A. Olsson, Auroral potential structures and current-voltage relationship: Summary of recent results, *Phys. Chem. Earth*, 1–3, 26, 107–111, 2001.

[18] Janhunen, P., A. Olsson, and H. Laakso, Altitude extension of auroral potential structures by event-based and statistical studies, *Adv. Space Res.*, in press, 2001.

[19] Janhunen, P., A. Olsson, and H. Laakso, A hybrid simulation model for a stable auroral arc, *Ann. Geophys., 20*, 1603-1616, 2002.

[20] Janhunen, P., and A. Olsson, The occurrence frequency of auroral potential structures and electric fields as a function of altitude using Polar/EFI data, *Ann. Geophysicae,* submitted, 2002.

[21] Janhunen, P., A. Olsson, and W.K. Peterson The occurrence frequency of upward ion beams in the auroral zone as a function of altitude using Polar/TIMAS and DE-1/EICS data, *Ann. Geophysicae,* in press, 2003.

[22] Janhunen, P., A. Olsson, and H. Laakso Middle-energy electron anisotropies in the auroral region, *Ann. Geophysicae,* submitted, 2003.

[23] Janhunen, P., A. Olsson, and H. Laakso Altitude dependence of plasma density in the auroral zone, *Ann. Geophys.*, ,, 20, 1743-1750, 2002.

[24] Janhunen, P., A. Olsson, A. Vaivads and W.K. Peterson, Generation of Bernstein waves by ion shell distributions in the auroral region, *Ann. Geophysicae,* in press, 2002.

[25] Kletzing, C.A. and J.D. Scudder, Auroral-plasma sheet electron anisotropy, *Geophys. Res. Lett., 26*, 971–974, 1999.

[26] Mälkki, A., A.I. Eriksson, P.O. Dovner, R. Boström, B. Holback, G. Holmgren and H.E.J. Koskinen, A statistical survey of auroral solitary waves and weak double layers: 1: Occurrence and net voltage, *J. Geophys. Res.*, 98, 15521–15530, 1993.

[27] McIlwain, C.E., Direct measurement of particles producing visible aurora, *J. Geophys. Res., 65*, 2727, 1960.

[28] Mozer, F.S. and A. Hull, Origin and geometry of upward parallel electric fields in the auroral acceleration region, *J. Geophys. Res., 106*, 5763–5778, 2001.

[29] Olsson, A. and P. Janhunen, A statistical study of nightside inverted-V events using Freja electron data: Implications for the current-voltage relationship, *J. Atmos. S. Terr. Phys.*, 62, 81–92, 2000.

[30] Olsson, A. and P. Janhunen, Difference in the current-voltage relationships between dawn and duskside inverted-V events, *J. Geophys. Res., 105*, 5373–5380, 2000.

[31] Olsson, A., Janhunen, P., H. Laakso, A. Vaivads Broadband 1-10 Hz waves in the auroral region, *Ann. Geophys.*, ,, submitted, 2003.

[32] Papadopoulos, K., A review of the anomalous resistivity for the ionosphere, *Rev. Geophys. Space Phys.*, 15, 113, 1977.

[33] Russell, C.T., R.C. Snare, J.D. Means, D. Pierce, D. Dearborn, M. Larson, G. Barr and G. Le, The GGS/Polar Magnetic Fields Investigation, *Space Sci. Rev.*, 71, 563–582, 1995.

[34] Scudder, J.D., *et al*., Hydra - A 3-dimensional electron and ion hot plasma instrument for the Polar spacecraft of the GGS mission, *Space Sci. Rev.*, **71**, 459-495, 1995.

[35] Shelley, E.G., R.G. Johnson and R.D. Sharp, Satellite observations of an ionospheric acceleration mechanism, *Geophys. Res. Lett., 3*, 654-656, 1976.

[36] Shelley, E.G., D.A. Simpson, T.C. Saunders, E. Hertzberg, H. Balsiger and A.G. Ghielmetti, The energetic ion composition spectrometer (EICS) for the Dynamics Explorer-A, *Space Sci. Instrum.*, 5, 443, 1981.

[37] Shelley, E.G., A.G. Ghielmetti, H. Balsiger, R.K. Black, J.A. Bowles, R.P. Bowman, O. Bratschi, J.L. Burch, C.W. Carlson, A.J. Coker, J.F. Drake, J. Fischer, J. Geiss, A. Johnstone, D.L. Kloza, O.W. Lennartsson, A.L. Magoncelli, G. Paschmann, W.K. Peterson, H. Rosenbauer, T.C. Sanders, M. Steinacher, D.M. Walton, B.A. Whalen and D.T. Young, The Toroidal Imaging Mass-Angle Spectrograph (TIMAS) for the Polar Mission, Space Science Rev., 71, 1-4, 1995.

[38] Stenbaek-Nielsen, H.C., T.J. Hallinan, D.L. Osborne, J. Kimball, C. Chaston, J. McFadden, G. Delory, M. Temerin and C.W. Carlson, Aircraft observations conjugate to FAST: auroral arc thickness, *Geophys. Res. Lett., 25*, 2073–2076, 1998.